First Observations with the UMass Dual-Beam InSAR

William N. Junek, Arunachalam Ramanathan,
Gordon Farquharson, Stephen J. Frasier,
Russell Tessier and David J. McLaughlin
Electrical and Computer Engineering
University of Massachusetts
Amherst, MA 01003
Email: frasier@mirsl.ecs.umass.edu

Mark A. Sletten and Jakov V. Toporkov
Naval Research Laboratory
Washington DC, 20375
Email: mark.sletten@nrl.navy.mil

***Abstract*— An dual-beam along-track interferometric synthetic aperture radar which is self contained within an aircraft pod has been developed to study coastal regions. System hardware is described. Initial test flights aboard the NOAA WP-3D research aircraft were performed to evaluate system performance over land and water surfaces. Notable look-angle dependences are observed in the sea surface NRCS under very low wind conditions.**

I. Introduction

Synthetic aperture radar has long been a tool for remote sensing of the ocean surface. Since the late 1980s, along-track synthetic aperture radar interferometry has been applied to numerous sea surface wave and current studies. Along-track interferometry employs two radar antennas separated in the along track direction to obtain the line-of-sight component of velocity of scatterers within the radar beam. An extensive review of SAR interferometry discussing both cross-track and along-track techniques is given in [1].

A logical extension of along-track interferometry is to employ two squinted beams to obtain two components of velocity [2], [3]. The Dual-Beam Interferometer (DBI) described in this paper is a C-band SAR designed to enable estimates of the ocean surface current vector with a single pass of an aircraft. All radar electronics and data acquisition are contained within a wing-mounted pod. The pod represents a convenient and economical platform for airborne remote sensing.

In this paper we describe the instrument hardware and airborne pod interface. We present dual-look SAR imagery over both land and water features obtained during initial engineering test flights. We do not show interferometric results, as such data have not yet been collected. The following sections describe respectively the instrument hardware, engineering test flight conditions, and sample imagery obtained.

II. System Description

A photograph of the DBI radar system is shown in Fig. 1. In its present configuration, it consists of two pairs of squinted antennas, a pulse-compression radar transceiver, a data acquisition and control system, and a velocity/attitude measurement system.

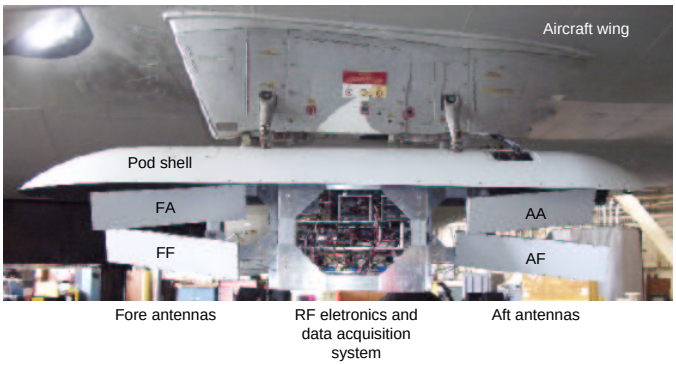

Fig. 1. Photo of DBI installed on WP-3D wing pylon. The lower section of the pod is removed.

Each interferometer consists of a pair of C-band microstrip patch array antennas separated by a baseline of 1.1 m. The antennas are designated by location (fore or aft) and orientation (fore or aft). Thus FF is the forward-located, forward-squinted antenna; FA is the forward-located, aft-squinted antenna, and so on (see Fig. 1). Antennas FF and AF comprise the forward looking interferometer while antennas FA and AA comprise the aft-looking interferometer. For each interferometer, the forward antenna transmits and receives while the aft receives only. As a result, the effective along-track baseline is half the physical baseline. The antennas are vertically polarized with half-power beamwidths of 7° (H-plane) and 31° (E-plane). The antennas are oriented towards 70° incidence and 20° squint angles.

A linear FM chirp waveform is generated by a direct digital synthesizer (DDS) and upconverted to 5.3 GHz and transmitted through one of the fore antennas. A pair of receivers connected to both fore and aft antennas demodulate the received signals using an intermediate frequency of 300 MHz. Each receiver produces in-phase and quadrature outputs for the data acquisition system. An internal calibration loop permits periodic monitoring of the transmitted chirp signal. Table I lists typical system parameters.

The radar also integrates GPS/INS information into the

TABLE I
DBI PARAMETERS

Parameter	Specification
Center Frequency	5.3 GHz
Polarization	VV
Bandwith	5-25 MHz
Pulse width	10 μs
Pulse repetition frequency	12 KHz
Transmitted power	50 W
Receiver noise figure	3 dB
Platform height	1000 m
Platform velocity	100 m/s
Antenna Baseline	1 m
Boresight incidence angle	70°
Squint angle	20°
Azimuth Beamwidth	7°
Elevation Beamwidth	30°

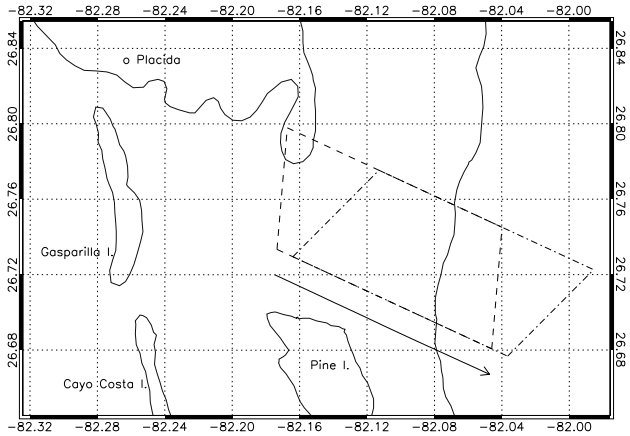

Fig. 2. Flight path corresponding to the images in Fig. 3. The forward (dash-dot) and aft (dash) antenna swath projections are shown.

data stream. Attitude/position information is provided by a Boeing CMIGITS-II, a digital quartz inertial measurement unit (DQI) with a 5-channel, L1 Coarse/Acquisition (C/A) code GPS engine. The system also accepts differential GPS corrections provided by the U.S. Coast Guard network of 300 kHz beacons.

Data acquisition is provided by a pair of custom boards developed at the University of Massachusetts [4]. These incorporate two 12-bit 65 MSPS analog to digital converters each followed by real-time coherent integration and dual IDE disk interfaces. The coherent integrator and disk interface are implemented using a pair of field programmable gate arrays (FPGAs), and the board is controlled by an ARM microprocessor which can also access data in shared memory on the board and which communicates via a serial port or Ethernet interface. The system currently supports sustained data rates to disk of 6 MB/s per receiver. With 320 GB of onboard storage, the system can acquire up to 14 hours of data between backups.

The radar is housed within a composite instrument pod that is mounted to a fixed pylon located under the wing of the aircraft. The pod payload area is approximately 1.5 m in length with a 60 cm diameter and supports a load of up to 120 kg. The payload is rigidly attached to the upper section of the pod as shown in Fig. 1 while the lower section serves as an aerodynamic radome consisting of a woven composite material (SpectraVue) with a nomex core.

The pod obtains 400 Hz power from the aircraft engines through the mating pylon. All other communications and control are performed via a 2.4 GHz wireless interface to the operator in the fuselage. Only a laptop equipped with a wireless interface is required within the aircraft.

III. INITIAL RESULTS

During Dec 2002, initial test flights aboard the NOAA WP-3D research aircraft were performed from the NOAA Aircraft Operations Center in Tampa, FL. The pod was mounted on the left wing of the aircraft inboard of the engines. Test flights were flown on 13 Dec 2002, and 17 Dec 2002. A few installation constraints precluded full system testing. Data were collected only for antennas FF and FA corresponding to forward and aft looks from the forward pair of antennas.

Fig. 3 shows a transect over Charlotte Harbour, south of Port Charlotte, WNW of Ft. Myers, FL. The flight path is superimposed on a map of the area in Fig. 2. Both forward and aft beams are shown. Given the very low surface winds, flight altitude was approximately 600 m. The swath corresponds to incidence angles between 69° and 86° and the swath width is approximately 7 km resolved with moderate resolution of 16.7 m in range. Images were focused using an adaptation of the extended chirp scaling algorithm [5] implemented by NRL. Range and azimuth resolution are approximately matched with 66 independent looks.

Sinuous surface slick features are observable over much of the water surface within the bay. Such features are commonly observable under light surface winds and are often attributed to biological sources (e.g. [6], [7]). The surface film modifies the surface tension of the water, suppressing the Bragg-resonant capillary waves responsible for the microwave echo.

We note a distinct difference in ocean backscatter intensity between the forward and aft looks. Having equalized the range dependent intensity variation over land, we find that features on the ocean surface are more distinct in the forward look. Given the similar intensities of land echos, it is likely that these differences are a consequence of the directional spectrum of Bragg resonant surface waves. In images from the same transect, an ocean front was clearly observed in the forward look where in the aft look it was nearly indistinguishable.

IV. SUMMARY

In this paper we have described a newly constructed dual-beam SAR which operates within a wing-mounted aircraft pod. Initial test flights aboard NOAA's WP-3D research aircraft demonstrated the functionality of the system. SAR images of ocean surface slicks and the angular dependence of radar backscatter over land and water were presented.

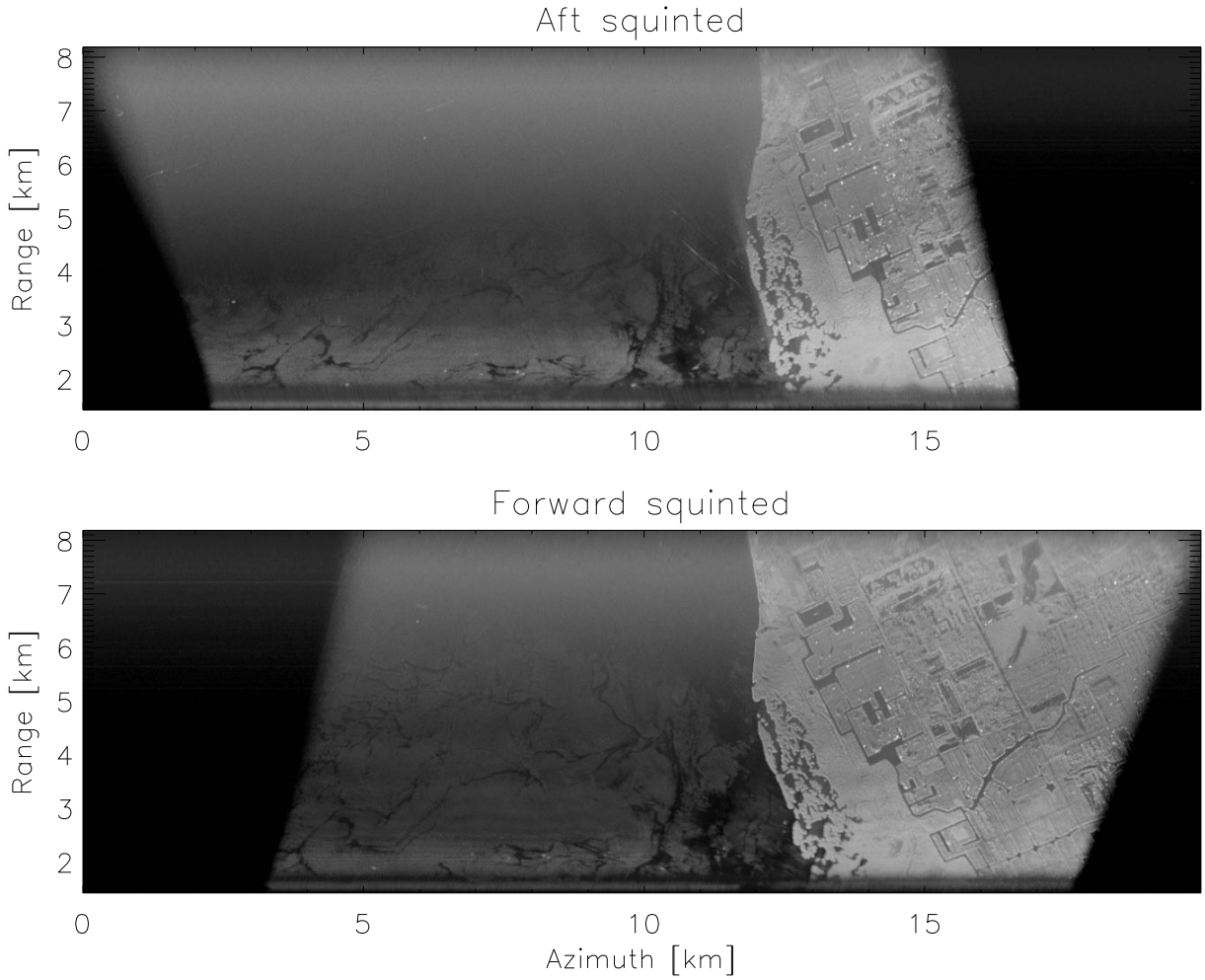

Fig. 3. Forward and aft antenna SAR images. The length of the data segment is 150 seconds which at an average speed of 93 m/s corresponds to an along-track range of 13.95 km. The altitude for this pass was approximately 590 m.

ACKNOWLEDGMENT

The authors gratefully acknowledge the generous logistical and technical support of the NOAA Aircraft Operations Center in Tampa, FL. This work was funded by the Office of Naval Research, Remote Sensing and Space Program [N00014-98-1-0612] and through the Physics of INSAR-Based Ocean Surface Current Measurement Program at the Naval Research Laboratory.

REFERENCES

[1] P. Rosen, S. Hensley, I. R. Joughin, F. K. Li, S. N. Madsen, E. Rodriguez, and R. M. Goldstein, "Synthetic aperture radar interferometry," *Proc. IEEE*, vol. 88, no. 3, pp. 333–382, Mar. 2000.

[2] E. Rodriguez, D. Imel, and B. Houshmand, "Two-dimensional surface currents using vector along-track interferometry," in *Proc. PIERS'95*, Seattle, WA, 1995, p. 763.

[3] S. Frasier and A. Camps, "Dual-beam interferometry for ocean surface current vector mapping," *IEEE Trans. Geosci. Remote Sensing*, vol. 39, no. 2, pp. 401–414, Feb. 2001.

[4] A. Ramanathan, "Acquisition of sensing data on a reconfigurable platform," Master's thesis, University of Massachusetts, Amherst, MA, Feb. 2003.

[5] A. Moreira and Y. H. Huang, "Airborne SAR processing of highly squinted data using a chirp scaling approach with integer motion compensation," *IEEE Trans. Geosci. Remote Sensing*, vol. 32, no. 5, pp. 1029–1040, Sept. 1994.

[6] A. R. Ochadlick, P. Cho, and J. Evansmorgis, "Synthetic aperature radar observations of currents colocated with slicks," *J. Geophys. Res.*, vol. 97, no. C4, pp. 5325–5330, Apr. 1992.

[7] G. O. Marmorino, D. R. Lyzenga, and J. A. C. Kaiser, "Comparison of airborne synthetic aperture radar imagery with in situ surface-slope measurements across gulf stream slicks and a convergent front," *J. Geophys. Res.*, vol. 104, no. C1, pp. 1405–1422, Jan. 1999.